In-situ Construction of a Hybrid Interfacial Protective Layer for Highly Stable Li Metal Anodes

Shunqiong Jiang[1,2], Wei Ying Lieu[2,3], Xue Liang Li[2], Daliang Fang[2], Siew Lang Teo[3], Yifan Li[2], Zhi Wei Seh[3], Bingbing Tian[1]*, Yumeng Shi[1]*, Hui Ying Yang[2]*

1. International Collaborative Laboratory of 2D Materials for Optoelectronics Science and Technology of Ministry of Education, Institute of Microscale Optoelectronics, Shenzhen University, Shenzhen 518060, P. R. China

2. Pillar of Engineering Product Development, Singapore University of Technology and Design, 8 Somapah Road, 487372, Singapore

3. Institute of Materials Research and Engineering (IMRE), Agency for Science, Technology and Research (A*STAR), 2 Fusionopolis Way, Innovis #08-03, Singapore 138634, Republic of Singapore

Abstract: Lithium (Li) metal is an ideal anode candidate for rechargeable batteries because of its ultra-high theoretical specific capacity. Unfortunately, the practical application of Li metal anodes is severely limited by the uncontrollable formation and growth of dendrites and infinite volume expansion. Thus, a protective layer is essential for stable and high-performance Li metal anodes. In this work, we demonstrate an organic-inorganic hybrid interfacial protective layer on Li foil surface (pa-Li) consisting of the organic PVDF-HFP and inorganic Ag-Li_xAg_y composite species. Going beyond conventional protective layers, we demonstrate that our hybrid protective layer is flexible and enabled strong interfacial adherence due to an alloying process. Furthermore, owing to the protective layer's outstanding lithiophilicity and mechanical stability, the pa-Li ‖ pa-Li symmetric cell exhibits satisfactory stability and reversibility for 1000 h at 5 mA cm^{-2}, 5 mA h cm^{-2} with a low voltage hysteresis of ~ 70 mV, while the full cell with a $LiFePO_4$ cathode delivers an excellent reversible capacity of 128.9 mA h g^{-1} for 900 cycles at 2 C with a capacity decay rate of 0.009% per cycle. This work proposes a design protocol for synergistic effect of PVDF-HFP organic species and Ag-Li_xAg_y inorganic species and provides a prospective way to practical application of highly efficient, long lifespan Li metal batteries.

Keywords: Li metal anode, organic-inorganic composite, protective layer, interfacial structure, Li metal batteries

1. Introduction

The rapid development of portable electronics and electronic vehicles has put forward great requirements for high-energy-density energy storage system.[1-3] The Lithium (Li) metal anode has been recently regarded as the most promising negative electrode material due to its high theoretical specific capacity (3860 mA h g^{-1}) and the lowest electrode potential (−3.04 V versus standard hydrogen electrode).[4-6] However, the practical application of Li metal anode is greatly hindered by its poor cycle performance and safety issues deriving from dendritic growth and side reactions.[7-16]

To handle the issues of Li metal anode, numerous methods have been adopted to suppress the growth of Li dendrite and inhibit the side reactions between Li metal anode and electrolyte. These methods include having a 3D conductive host design,[17-20] separator modification,[21-24] electrolyte engineering,[25-28] and protective layer construction.[29-32] Amongst these approaches, constructing protective layer is regarded as an effective method to inhibit the growth of Li dendrites and improve the stability of Li metal anode.[33-35] The method of constructing an artificial protective layer on Li foil has attracted much attention due to the following advantages: i) it homogenizes the Li^+ ion flux through the protective layers to Li foil surface, resulting in uniform Li deposition; ii) side reactions between the electrolyte and Li metal can be reduced as solvent or anion molecules are isolated by the coated protective layer; iii) suitable mechanical properties of the protective layer can prevent the deposited Li from penetrating through the separator. Therefore, effective protective layers can avoid the growth of Li dendrites and formation of "dead Li", enabling the stable and safe Li metal

batteries.

To suppress Li dendrite growth and avoid corrosion of the Li foil, the protective layer should ideally have good electrochemical stability and mechanical properties.[36-38] A high ionic conductivity is also crucial for good electrochemical performance.[39-40] In previous reports, there are two main material engineering categories for protective layers: organic or inorganic materials. For organic layers (e.g., PVDF and PDMS), they have excellent flexibility, thus alleviating volume expansion during Li deposition.[41-42] For inorganic layers (e.g., Li-wetting metals or Li-based alloys), they have good mechanical strength to inhibit Li dendrite from piercing through the separator.[43-44] However, it is difficult for Li anodes with only organic or inorganic protective layer to achieve satisfactory stability. Inorganic layers are known to exhibit excellent chemical stability when used with a Li metal anode. However, their rigid nature makes them susceptible to cracking and failure of the protective layer due to the significant volume changes that occur during cycling. In contrast, organic protective films are more elastic, which helps to avoid the issues associated with inorganic layers, which enhances their long-term protective properties for Li metal anodes, whereas protective layers based only on organic species will result in poor interfacial contact with Li foil, and the cracks will appear after long-term cycling because of low strength of organic films.[45] Such cracks and poor interfacial contact will inevitably compromise the commercial viability of such protective layers. Therefore, there is a need to develop a protective layer with not just good ionic conductivity, lithiophilicity and excellent electrochemical stability, but also particularly with high mechanical modulus and strong interfacial adhesion

properties. There are a few reports focused on the construction of hybrid protective layer, showing some satisfactory results.[46] However, the evolution of interfacial structure has rarely been explored to explain the failure of the protected Li foil, warranting further in-situ studies in this direction.

In this work, we designed and synthesized an interfacial protective layer with organic (PVDF-HFP) and inorganic (Ag-Li_xAg_y) composite species on Li foil (pa-Li) for dendrite-free and highly stable Li metal anode. Ag and Li_xAg_y are known to have excellent lithium wettability and undergoes an alloying process, which is beneficial to uniform Li deposition,[47-48] whereas PVDF-HFP has good ionic conductivity, flexibility, and compatibility. This hybrid interfacial protective layer can be synthesized in-situ on Li foil surfaces easily, aiding in potential future mass production. In-situ optical microscopy is also used to observe the morphology evolution on Li foil surface during the plating process. Thus, owing to its outstanding Li ion conductivity and excellent mechanical properties, the pa-Li foil achieves dendrite-free Li plating/stripping behaviors and superior long-term cycling stability. Consequently, the pa-Li||pa-Li symmetric cell exhibits satisfactory stability and reversibility for 1000 h at a high current density of 5 mA cm^{-2}, 5 mA h cm^{-2} with a low voltage hysteresis of ~ 70 mV. In addition, the full cell with pa-Li anode and a commercial $LiFePO_4$ cathode delivers an impressive reversible capacity of 128.9 mA h g^{-1} for 900 cycles at a current density of 2 C, with a low capacity decay rate of 0.009% per cycle. Therefore, the hybrid Li foil protective layer enables the synergistic effect of PVDF-HFP organic species and Ag-Li_xAg_y inorganic species to be exhibited through a strong interfacial adherence and

provides a prospective way for the practical application of highly efficient, long lifespan Li metal batteries.

2. Experimental Section

Chemicals and Materials: The Li foil with 16 mm of diameter and 500 μm of thickness was purchased from China Energy Lithium Co., Ltd. $AgNO_3$ (99%), PVDF-HFP (average M_w ~400,000, average M_n ~130,000, pellets) and NMP (99%) were purchased from Sigma-Aldrich Co, Ltd.

Preparation of a-Li, p-Li and pa-Li: The preparation process of protected Li anode was operated in an argon-filled glove box (O_2 < 0.1 ppm, H_2O < 0.1 ppm). First, 8.5 mg of $AgNO_3$ (10 mM) and 250 mg PVDF-HFP were dissolved in 5 mL 1-Methyl-2-pyrrolidinone (NMP) to get a mixture solution. Then, 50 μL of mixed solution was dripped onto the surface of the Li foil, flowing to the fully cover the Li foil, followed by an in-situ sedimentation process at 80 ℃ for 24 h ($Li + Ag^+ \rightarrow Li^+ + Ag$, $xLi + yAg \rightarrow Li_xAg_y$) until the solvent completely evaporated to obtain the protected Li foil with PVDF-HFP and Ag-Li_xAg_y composite protective layer (pa-Li). For comparison, the protected Li foil with only Ag-Li_xAg_y (a-Li) or PVDF-HFP (p-Li) protective layer was prepared by similar method.

Materials characterization: The microstructures and X-ray energy-dispersive spectrometer (EDS) were confirmed by field emission scanning electron microscopy (FESEM, JSM-7600F; JEOL, Japan). The crystal structure of bare Li, a-Li, p-Li and pa-Li were investigated by a Bruker D8 Avance X-ray diffractometer equipped with Cu Kα radiation (λ = 0.154 nm). The X-ray photoelectron spectroscopy (XPS) was

performed on PHI, Model 5600, with monochromatic Al Kα X-rays (350 W) and a pass energy of 29 eV.

Electrochemical measurement: All the electrochemical tests were carried out with CR2032-type coin cells, which were assembled in an argon-filled glove box (O_2 < 0.1 ppm, H_2O < 0.1 ppm) by using Celgard 2400 as the separator. The symmetric cells were assembled with different Li anodes (bare Li, a-Li, p-Li and pa-Li) and 50 μL of 1.0 M lithium bis(trifluoroethanesulfonate)imide (LiTFSI) and 2 wt% $LiNO_3$ in DOL/DME (volume ratio, 1:1) mixed solvent as the electrolyte. The galvanostatic cycling tests were carried out at different current density with different areal capacity on a Neware battery testing system.

Full cells were assembled with $LiFePO_4$ (LFP) as cathode and different Li foils as anodes. LFP cathodes were prepared by casting NMP slurry containing $LiFePO_4$ active material, carbon black, and poly (vinylidene difluoride) (PVDF) with a weight ratio of 8:1:1 onto the Al foil. After drying in a vacuum oven at 80 ℃ for 12 h, the electrodes were punched to disks of 10 mm in diameter. The Li ‖ LFP coin cells were assembled with carbonate-based electrolyte (1.0 M $LiPF_6$ in EC/DEC with the ratio of 1:1 by volume). And the voltage window for the full cell is set at 2.5–3.8 V. All electrostatic discharge/charge measurements were operated by a multi-channel battery test system (Neware, Shenzhen, China). The electrochemical impedance spectrometry (EIS) analysis was conducted by a VMP3 electrochemical workstation with the frequency range of 100 kHz to 0.01 Hz.

In situ optical cell observation: For the in situ optical test, rectangular Li flakes

(0.5×2 cm^2) were cut from bare Li, a-Li, p-Li and pa-Li foils and symmetric cells were assembled in a transparent quartzose cell with 5 mL electrolyte (1.0 M LiTFSI and 2 wt% $LiNO_3$ in 1:1 volume ratio of DOL/DME). All the operations were carried out in the glove box (O_2 < 0.1 ppm, H_2O < 0.1 ppm). The cells were galvanostatic cycled (5 mA cm^{-2}, 5 mA h cm^{-2}) by using a Neware battery test system. Meanwhile, the display-connected microscope recorded the morphology evolution of the Li metal anodes during the Li plating process through the transparent quartzose cells.

3. Results and Discussion

The synthesis process of Li metal anode with organic-inorganic composite protective layer is illustrated in **Figure 1**a. The protective layer was constructed by a drip-casting method. First, 50 μL of the mixed solution ($AgNO_3$ and PVDF-HFP in NMP) was dropped on the surface of Li foil and shaken gently to allow the mixture to completely cover the surface. Then, the treated Li foil was heated at 60 ℃ for 24 h to realize an in-situ ion-exchange and alloying reaction, followed by the sedimentation of organic species. Finally, the Li metal anode with organic-inorganic composite protective layers was obtained and denoted as pa-Li. For comparison, a-Li and p-Li samples were prepared by a similar method using solution containing only either $AgNO_3$ or PVDF-HFP respectively.

Figure S1 and **Figure 1**b show the top-view morphologies of bare Li, a-Li, p-Li and pa-Li, which were vastly different from the bare surface of pure Li foil (Figure S1a). The SEM image of a-Li clearly review a crude surface deposited with a large number of particles (Figure S1b). The top-view SEM images of the as-synthesized p-Li and pa-

Li show a uniform scale-like surface (**Figure 1**b and Figure S1c) due to the presence of the PVDF-HFP film. The corresponding energy dispersive spectroscopy (EDS) mapping results indicate a homogeneous distribution of F, Ag elements (**Figure 1**c, d). The EDS mapping of a-Li (N, O, Ag elements) and p-Li (C, F elements) are shown in Figure S2 a, b.

To determine the interfacial compatibility between the protective layer and Li foil, a thorough analysis based on focused ion beam-scanning electron microscopy (FIB-SEM) was carried out. **Figure 1**e show the cross-sectional view of the pa-Li with two completely connected layers. It was observed that a dense protective layer of ~ 4 μm is formed on the surface of lithium foil after in-situ reaction and sedimentation. The SEM images of cross-sectional view of bare Li, a-Li and p-Li are shown in Figure S3. There is no protective layer of bare Li according to the cross-section morphology as shown in Figure S3a. The a-Li has a compact Ag-Li_xAg_y layer on the surface of Li foil (Figure S3b), while a little gap appears between PVDF-HFP layer and Li foil in p-Li (Figure S3c) because of the solvent evaporation during the synthesis process. The corresponding EDS mapping results of pa-Li's cross-sectional view indicate a homogeneous distribution of C, N, O, F and Ag (Figure S4). Apart from the characteristic peaks of metallic Li and Ag, the characteristic peaks of Li_xAg_y also appeared in both the XRD patterns of a-Li and pa-Li (**Figure 1**f, Figure S 5a). This is in contrast with the XRD patterns of bare Li and p-Li, in which only the characteristic peaks of metallic Li were observed. (Figure S5b, c). This indicates that alloying occurs between the Li and Ag metals of a-Li and pa-Li. As shown in **Figure 1**g, the spectra of

Ag 3d can be resolved into two peaks, in which the peaks at 367.2 eV and 372.7 eV can be fitted into Ag $3d_{5/2}$ and Ag $3d_{3/2}$, respectively, proving the existence of metallic Ag. Moreover, XPS with Ar^+-ion sputtering was used to analyze the chemical state in depth. With further sputtering, the peaks of Ag $3d_{5/2}$ and Ag $3d_{3/2}$ shift to higher binding energies (367.7 eV, 373.6 with 1 min etching; 368.2 eV, 374.3 eV with 5 min etching and 368.3 eV, 374.3 eV with 10 min etching), indicating the appearance of reduced Ag corresponding to the strong interaction between Ag and Li,[49-50] which suggests the formation of Li_xAg_y alloy, and is beneficial to the contact between Li foil and protective layer.

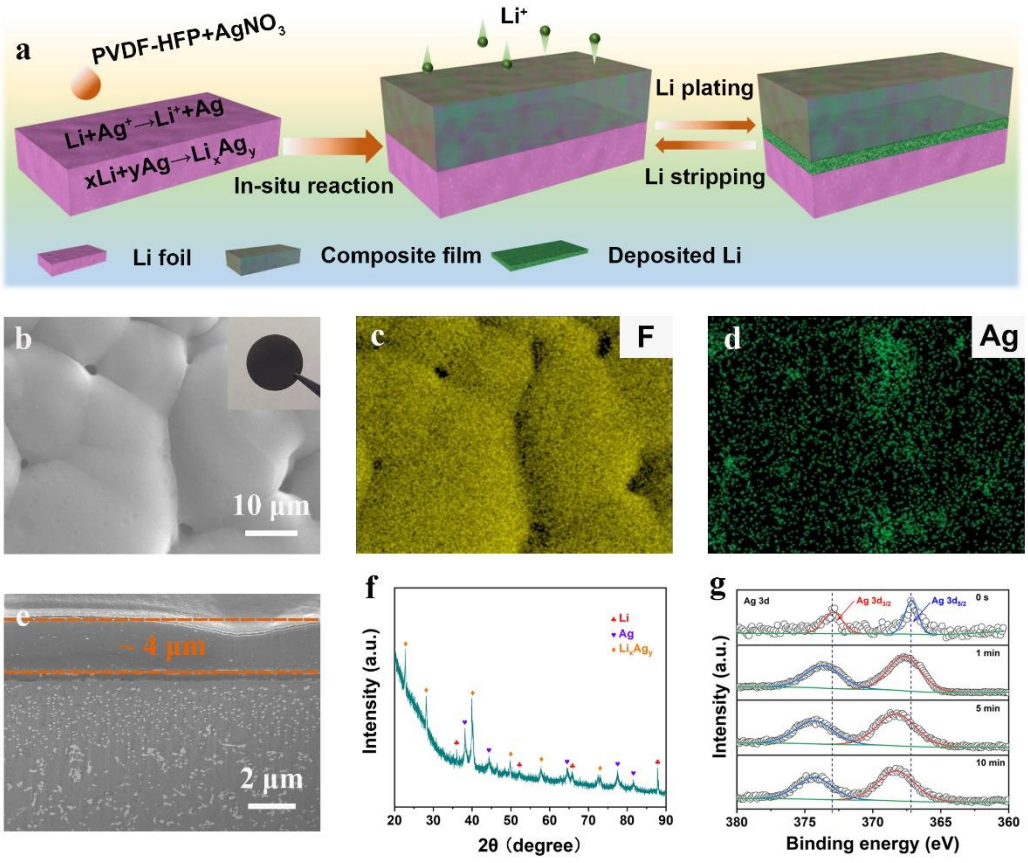

Figure 1. (a) Schematic illustration of the preparation process of pa-Li anode with organic-inorganic composite protective layer. (b) Top-view SEM image of pa-Li (insert

image is the digital photo of pa-Li foil) and (c, d) the corresponding EDS mapping images of F and Ag elements respectively. (e) Cross-sectional FIB-SEM image of pa-Li foil. (f) XRD pattern of pa-Li and (g) XPS spectra of Ag 3d with different etching time.

To investigate the advantages of organic-inorganic composite protective layer for Li metal anode, the electrochemical properties of bare Li, a-Li, p-Li and pa-Li were tested. The coulombic efficiency (CE) in the Li||Cu asymmetric cell is a key indicator of the long-term stability and reversibility of Li anodes. As shown in **Figure 2**a, the Li||Cu asymmetric cell with pa-Li anode delivers a high CE value of ~ 98.5% and excellent cycling stability for over 300 cycles, whereas the cell with bare Li suffered an unstable CE and performance degradation after 50 cycles. In contrast, the CE of the cell with a-Li and p-Li performed worse than the cell with pa-Li, but far better than the cell with bare Li. The cell with a-Li maintained a CE value of ~ 97.8% for 190 cycles before rapid CE decay, whereas the cell with p-Li could retain a CE of ~ 97.5% for nearly 220 cycles before CE decay. Therefore, the pa-Li||Cu asymmetric cell achieves the most excellent long-term stability and cyclic reversibility.

Electrochemical impedance spectroscopy (EIS) was further applied to compare the interfacial resistance and stability of the symmetric cells with different protective layers. According to the equivalent circuit model as shown in Figure S6, the R_s represents the intrinsic bulk resistance of cell. The $R_{interphase}$ and CPE_1 are the resistance and capacitance of the protective layer and/or the existing SEI layer, corresponding to the semicircle at the high-frequency region in EIS. The medium frequency region

represents the charge transfer resistance (R_{ct}) and double-layer capacitance (CPE_2). As shown in **Figure 2**b, the interfacial impedance of symmetric cell with p-Li (75.6 Ω) is lower than those of symmetric cells with a-Li (187.0 Ω) and pa-Li (117.2 Ω) before cycling because of the reaction between $AgNO_3$ and metallic Li to form some nonconductive inorganic species. After cycling for 40 h at 3 mA cm^{-2} with a areal capacity of 3 mA h cm^{-2}, the symmetric cells with a-Li, p-Li and pa-Li exhibited a large decrease in interfacial impedance, decreasing respectively to 10.2 Ω, 4.5 Ω and 2.5 Ω (**Figure 2**c). This indicates that a stable SEI is constructed on the surface of lithium foil, and a good transportation pathway of Li^+ ion was formed in the protective layer. However, for the symmetric cell with bare Li, the interfacial impedance kept increasing during the cycling process (cycled for 20 h, 40 h, 60 h and 80 h, Figure S7), which is in agreement with the thickening of the SEI induced by the repeated breakage and regeneration of a natural SEI. The results of the EIS reveal that the organic-inorganic composite film of pa-Li significantly improves the interfacial stability between lithium foil and electrolyte during the charge-discharge process, giving rise to much better Li^+ ion transport kinetics after the stable SEI established compared with bare Li and protected a-Li, p-Li.

To investigate the electrochemical properties of the Li anodes with different protective layer, galvanostatic cycling tests of symmetric cells were performed under various conditions, using an ether-based electrolyte (1 M LiTFSI in a 1:1 (v/v) mixture of DOL and DME, and 2 wt% $LiNO_3$ as additive). When cycling at a low current density of 0.25 mA cm^{-2} with a low areal capacity of 0.5 mA h cm^{-2}, the symmetric cell with

pa-Li anode displays a highly steady voltage-time profile with an overpotential of ~ 10 mV for over 1600 h. In contrast, the voltage-time profiles of the symmetric cells with a-Li and p-Li show unsteady with higher overpotential and shorter cycling time. For the symmetric cell with bare Li, the overpotential increased in the first 200 h and then decreased after 400 h, indicating cell failure due to an internal micro short circuit caused by Li dendrites and dead Li. When the current density and areal capacity have been risen to higher levels, the symmetric cells with protected Li anodes (a-Li, p-Li and pa-Li) still show lower overpotentials and better cycling stability compared with the symmetric cell with bare Li. Especially for the symmetric cells with pa-Li, it can maintain a stable electrochemical performance. The symmetric cells with pa-Li have the lowest overpotential for the longest cycling duration at 1 mA cm^{-2}, 1 mA h cm^{-2} (~ 19 mV, 1400 h) and 2 mA cm^{-2}, 2 mA h cm^{-2} (~ 27 mV, 1200 h). Even at 5 mA cm^{-2}, 5 mA h cm^{-2}, the symmetric cell with pa-Li is capable of stable electrochemical cycling for over 1000 h with a low overpotential of ~ 70 mV.

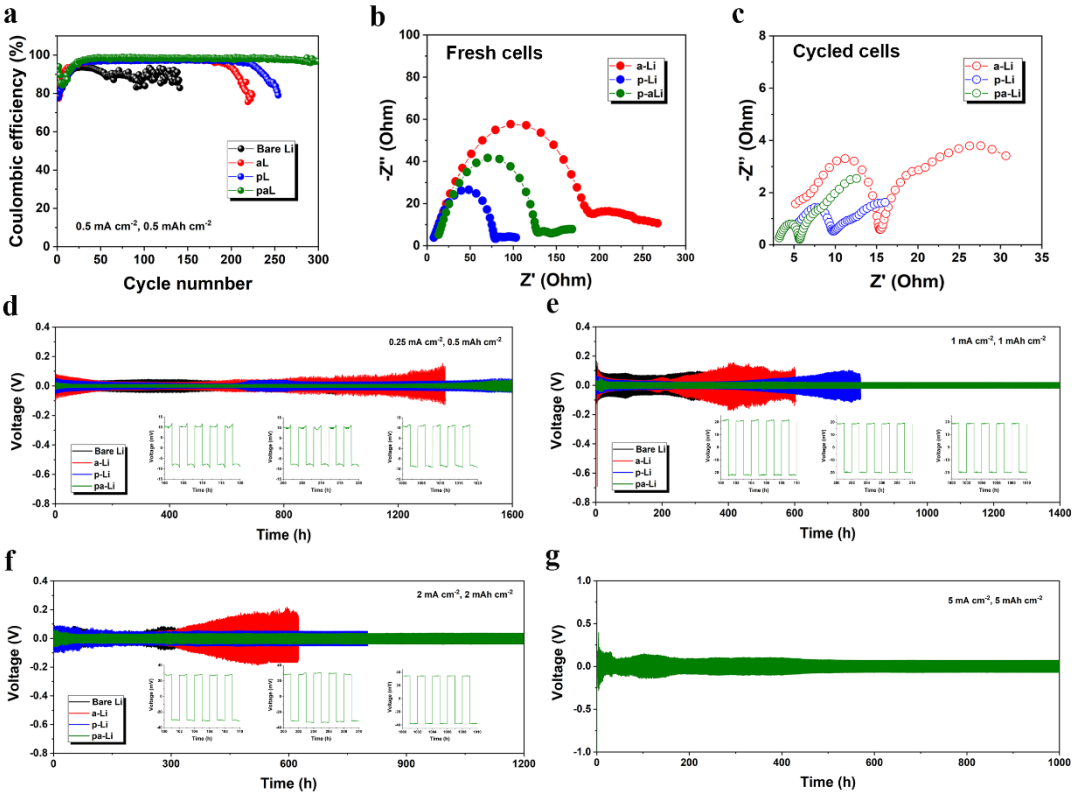

Figure 2. Electrochemical performance of Li metal batteries with bare Li, a-Li, p-Li and pa-Li anodes. (a) Coulombic efficiency of different Li | |Cu asymmetric cells for long-term cycles at 0.5 mA cm^{-2}, 0.5 mA h cm^{-2}. EIS profiles of different symmetric cells (b) before and (c) after cycling. (d-f) Voltage profiles of different symmetric cells at 0.25 mA cm^{-2}, 0.5 mA h cm^{-2}, 1 mA cm^{-2}, 1 mA h cm^{-2} and 2 mA cm^{-2}, 2 mA h cm^{-2}. (g) Voltage profiles of symmetric cells with pa-Li at 5 mA cm^{-2}, 5 mA h cm^{-2}.

As the symmetric cell with pa-Li has the lowest interfacial impedance and the best cycle performance, it indicates that there exists a stable surficial and interfacial structure between organic-inorganic composite film and Li foil. This was further demonstrated from the SEM images of bare Li, a-Li, p-Li and pa-Li after long-term cycling. In Figure S8a, it is observed that there is the much-pulverized substance on the bare Li foil corresponding to “dead Li”, suggesting unstable SEI and Li dendrites are formed during

the charge-discharge cycles. For a-Li anode, due to modulus mismatch between metallic Li foil and Ag or Li_xAg_y alloy, the Ag-Li_xAg_y composite layer obtained by in-situ reaction is prone to cracks. This resulted in the deposited metallic Li rupturing the Ag-Li_xAg_y composite layer, thus forming Li dendrites and an unstable SEI on surface (Figure S8b). Due to outstanding compatibility and flexibility of PVDF-HFP film, the morphology of the p-Li or pa-Li surface mostly remained unchanged after Li plating/stripping cycles. However, the deposited Li would pierce through the pure PVDF-HFP film with low mechanical strength, forming a small amount of "dead Li" (Figure S8c). Fortunately, the organic-inorganic composite film on the surface of pa-Li has high strength, so it can maintain stability well during Li plating/stripping process (Figure S8d). Figure S9 shows the mechanical properties of PVDF-HFP film and organic-inorganic composite film. A tensile strength (s) of 24.7 MPa and elongation at break (ε_b) of 206.8% are obtained for PVDF-HFP film, while the values of s and ε_b are 28.5 MPa and 143.3%. Based on the above, it is demonstrated that the introduction of inorganic species in PVDF-HFP film enhances the mechanical strength of composite film, which can better prevent the protective layer from being pierced through. Thus, the organic-inorganic composite film plays a crucial protective role for Li anode.

To further reveal the function of organic-inorganic composite protective layer, the interfacial structures of bare Li, a-Li, p-Li and pa-Li foils after long-term cycling in symmetric cells were studied by FIB-SEM (Figure S10). As shown in Figure S10a, there are many pores with different size in bare Li foil, indicating that volume expansion occurs in unprotected Li foil during Li plating/stripping process, resulting in the

formation of a porous and loose structure. For a-Li, the Ag-Li_xAg_y layer tend to be pulverized after the continuous Li^+ ion flux, resulting in the deposited lithium easily bursting out the protective layer (Figure S10b). For p-Li, because of the gap between the PVDF-HFP film and the Li foil, some tiny Li dendrites managed to appear on the surface of Li foil. This is detrimental to the longevity of the p-Li foil as the formation of internal dendrites further reduces and weakens the interfacial contact between the Li foil and the protective layer, eventually rendering the implementation of a protective layer useless. In contrast, the organic-inorganic pa-Li can maintain a compact structure without any pores. The existence of the Li_xAg_y alloy also enabled complete interfacial contact between the organic-inorganic composite film and the Li foil, thus preventing the formation of tiny dendrites. The schematic diagram of this Li plating/stripping process on the different Li foils is shown in Figure S11.

The excellent Li plating/stripping behaviors of pa-Li anode with an organic-inorganic composite protective layer can be also observed by in situ optical microscopy. To understand the deposition behavior of lithium metal, an in-situ optical system is used to observe and analyze evolution of morphology on lithium foil surface during plating process. In the optical cell as shown in Figure S12a, the gap (5 mm of width) between two pieces of bare or protected Li foils is filled with the electrolyte and there was no separator or applied pressure. The evolution of the structure and morphology on lithium foil surface were observed during plating process by the assembled optical cells (Figure S12b). **Figure 3** shows the evolution of the structure and morphology on the surface of bare Li, a-Li, p-Li and pa-Li during the Li plating process at a current density of 5 mA

cm^{-2}. The Li deposition on the bare Li foil started with inhomogeneous nucleation (15 min plating, **Figure 3**aii) before rapidly evolving into clusters of mossy Li scattered along the Li/electrolyte interface (30 min plating, **Figure 3a**iii). With further Li plating (45, 60 min plating, **Figure 3**aiv, v), these clusters eventually evolved into Li dendrites. In contrast, the surface of the protected Li foil (a-Li, p-Li or pa-Li) was smoother in the initial 15 min plating (**Figure 3**aii, bii, cii, dii), suggesting uniform Li^+ ion flux and Li nucleation. After prolonged plating, differences were observed in the structure and morphology of Li foils with different protective layers. For a-Li, tiny Li islands appeared after 30 min plating, indicating the deposited Li burst out the Ag-Li_xAg_y layer and Li^+ ion flux started to be plated on the surface. After 45 min and 60 min, more deposited Li appeared on the surface of a-Li and tend to form mossy Li and Li dendrites (**Figure 3**biv, v). It is also worth noting that a more uniform Li plating behavior was observed on p-Li or pa-Li surface. This uniform plating characteristic is particularly accentuated in pa-Li foil as the metallic Li can still be deposited uniformly after 45 min and 60 min of plating (**Figure 3**div, v). For p-Li foil, a small amount of mossy Li and tiny dendrites appear on the surface after prolonged plating (**Figure 3**civ, v), demonstrating that the deposited Li has pierce through the PVDF-HFP film. Thus, it can be concluded that the organic-inorganic composite protective layer is highly effective in alleviating the growth of Li dendrites and facilitating uniform Li deposition. Further optical images evolution of bare Li, a-Li, p-Li and pa-Li exposed to air for different time periods are shown in Figure S13. By comparison, it can be found that p-Li and pa-Li can remain chemically stable without significant color change when

exposed to air, whereas color change was observed on the surface of bare Li or a-Li. Given that Li metal is reactive in air, this evidence of the protective layers of p-Li and pa-Li effectively preventing direct contact between the Li foil surface and air is likely beneficial during mass production. Furthermore, it can be inferred that the protective layers of p-Li and pa-Li effectively prevent direct contact between the Li foil surface and the electrolyte, reducing the amount of side reactions occurring.

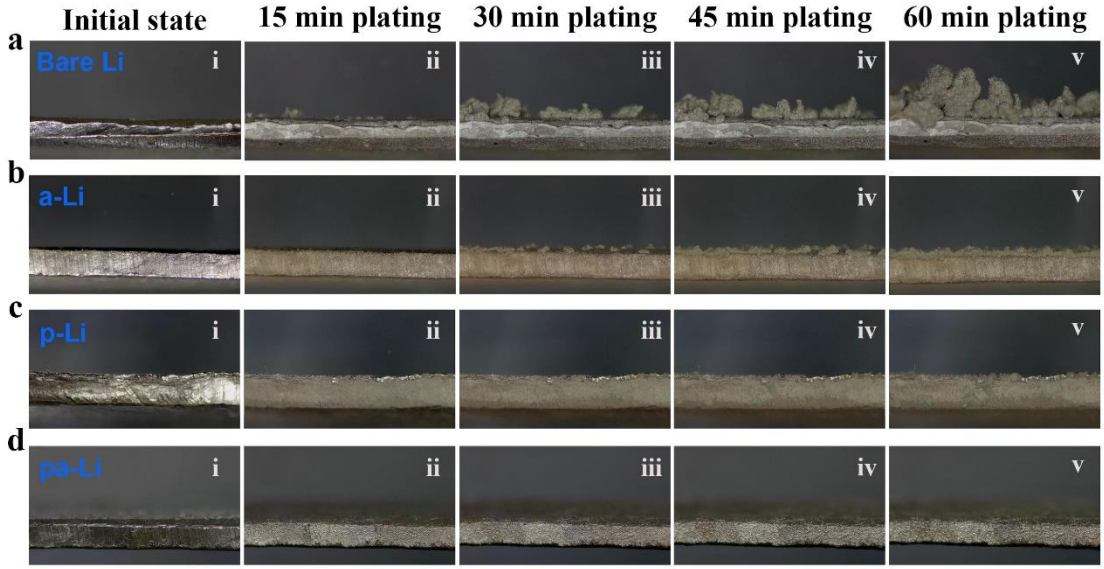

Figure 3. In-situ optical images of the electrode/electrolyte interfaces of (a) bare Li, (b) a-Li, (c) p-Li and (d) pa-Li during Li deposition at a current density of 5 mA cm^{-2}.

The SEM images of microtopography evolution on the surface of bare Li, a-Li, p-Li and pa-Li with different areal capacities are shown in **Figure 4**. After plating Li with the areal capacities from 1 mA h cm^{-2} to 10 mA h cm^{-2}, the deposited lithium tended to transform into Li dendrites on bare Li with the increase of deposition capacity (**Figure 4**ai-iii). This is in contrast with a-Li, in which lithium dendrites appeared on the surface just when the deposition capacity is 10 mA h cm^{-2} (**Figure 4**bi-iii), demonstrating that the Ag-Li_xAg_y protective layer can inhibit the growth of Li dendrites at low deposition

capacities. In contrast, the surface of p-Li and pa-Li can retain their initial morphologies after lithium plating, indicating Li^+ ions are deposited on the surface of Li foil below the protective layers (**Figure 4**ci-ciii, di-diii). In the stripping process, when the areal capacity decreased from 10 to 1 mA h cm^{-2}, metallic lithium was stripped uniformly from p-Li and pa-Li (**Figure 4**civ, div), while the flocculent and granular "dead Li" appeared on the surface of bare Li and a-Li (**Figure 4**aiv, biv). Therefore, PVDF-HFP layer or organic-inorganic composite layer of protected Li foil would improve the process of Li plating and stripping to inhibit the formation of Li dendrites and "dead Li".

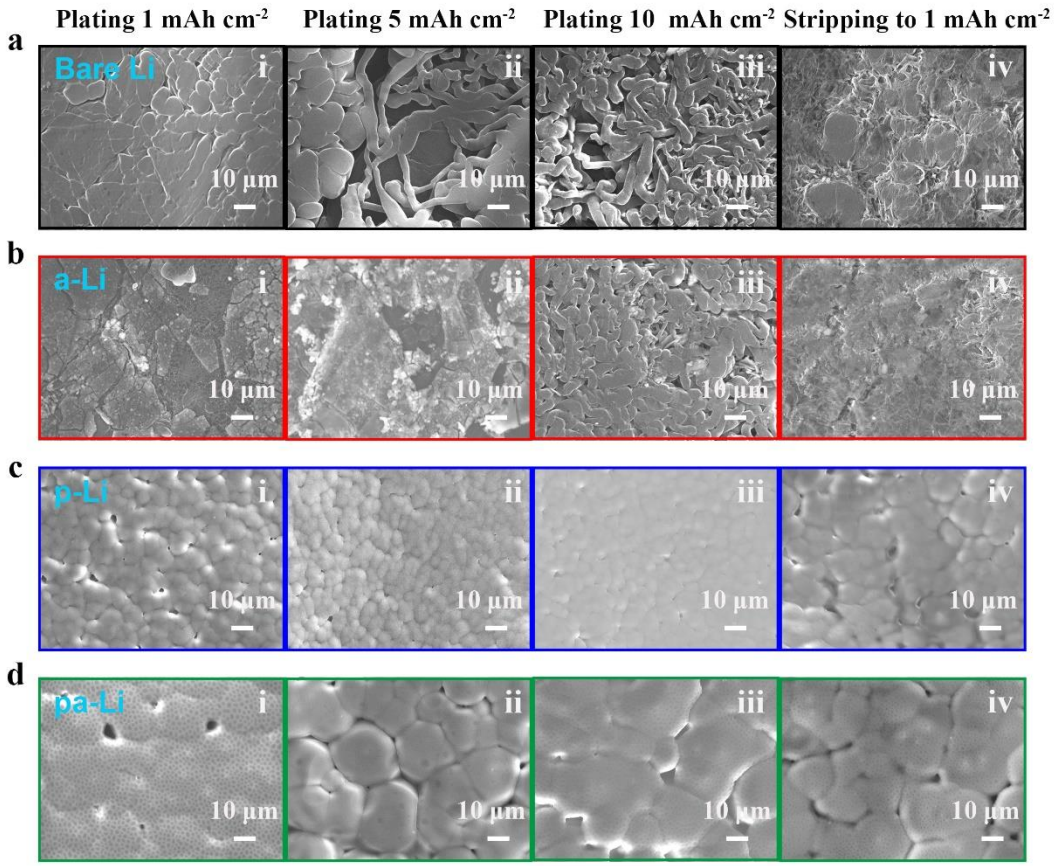

Figure 4. SEM images about morphology evolution of (a) bare Li, (b) a-Li, (c) p-Li and (d) pa-Li after Li plating with different capacities of (i) 1 mA h cm^{-2}, (ii) 5 mA h

cm^{-2} and (iii) 10 mA h cm^{-2}, and (iv) Li stripping to capacity of 1 mA h cm^{-2}.

Based on the excellent Li plating/stripping performance of pa-Li, the full cells with pa-Li as anodes and LFP as cathodes perform superior rate performance and outstanding long-term cycling stability. The rate capacities of different full cells with bare Li, a-Li, p-Li and pa-Li anodes (Li||LFP, a-Li||LFP, p-Li||LFP, pa-Li||LFP) are compared in **Figure 5**a. The pa-Li||LFP full cell delivers average reversible discharge capacities of ~ 167.7, 164.7, 157.3, 141.7 and 123.1 mA h g^{-1} at 0.1, 0.2, 0.5, 1 and 2 C, respectively, which are higher than these values of Li||LFP, a-Li||LFP, p-Li||LFP. The corresponding charge-discharge profiles of pa-Li||LFP full cell at various current densities are displayed in **Figure 5**b. In addition, the pa-Li||LFP full cell possesses a low polarization voltage, while there are higher values for Li||LFP, a-Li||LFP, p-Li||LFP full cells, demonstrating the boosted reaction kinetics. **Figure 5**c shows the voltage profiles of Li||LFP, a-Li||LFP, p-Li||LFP and pa-Li||LFP full cells at 1 C. It is observed that the pa-Li||LFP exists a highest specific capacity and lowest polarization voltage.

To further investigate the effectiveness of organic-inorganic composite protective layer, galvanostatic charge-discharge test was carried out to confirm the long-term cycling stability. **Figure 5**d shows the discharge capacity and CE of Li||LFP, a-Li||LFP, p-Li||LFP and pa-Li||LFP full cells at 1 C. Due to the organic-inorganic composite protective layer with high ion conductivity and excellent mechanical property, the pa-Li||LFP full cell realizes a superior long-term cycling performance which has a high initial discharge capacity of 144.0 mA h g^{-1} and keeps at 129.0 mA h

g^{-1} after 900 cycles with a low capacity decay of 0.012% per cycle. However, Li│ │LFP, a-Li│ │LFP and p-Li│ │LFP full cells suffer capacity decreasing quickly. When the current density is risen to 2 C, the pa-Li│ │LFP full cell also outperforms the Li│ │LFP, a-Li│ │LFP and p-Li│ │LFP full cells (**Figure 5**e). For the pa-Li│ │LFP full cell, the discharge capacity at the 1st cycle is 128.9 mA h g^{-1} and remains at 118.0 mA h g^{-1} after 900 cycles, delivering an extremely low capacity decay of 0.009% per cycle, whereas the Li│ │LFP, a-Li│ │LFP and p-Li│ │LFP full cells suffer fast capacity fading. The corresponding charge-discharge profiles at 1 C and 2 C of Li│ │LFP, a-Li│ │LFP, p-Li│ │LFP and pa-Li│ │LFP full cells are shown in Figure S14 and Figure S15. The SEM images of different Li foils in Figure S16a, e and Figure S16b, f show that the surface of the bare Li and a-Li are brittle and full of cracks due to the passivation/pulverization of the SEI and the accumulation of inactive lithium. Some cracks appear on the surface of PVDF-HFP protective film, with tiny inactive deposited Li (Figure S16c, g). In contrast, the pa-Li foil is smoother and no obvious cracks or pulverization species (Figure S16d, h). Thus, the satisfactory stability of organic-inorganic composite protective layer renders a long cycle life to the full cell.

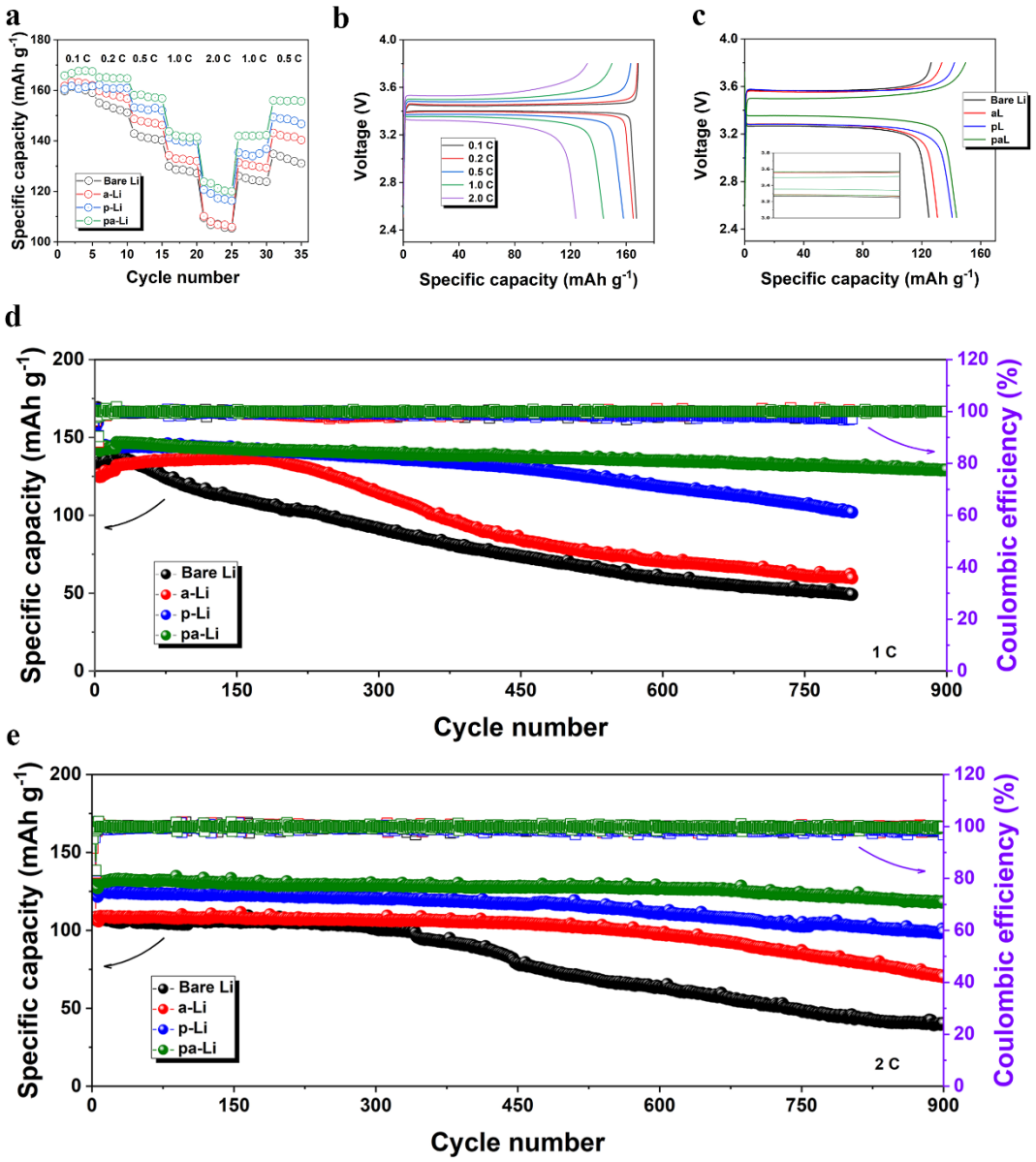

Figure 5. Electrochemical performance of Li||LFP, a-Li||LFP, p-Li||LFP and pa-Li||LFP full cells. (a) Rate performance of different full cells at current densities of 0.1, 0.2, 0.5, 1, 2 C. (b) Galvanostatic charge/discharge profiles at different current density of pa-Li||LFP full cell. (c) Galvanostatic charge/discharge profiles different full cells at a current density of 1 C. (d, e) Cycling performance and coulombic efficiencies of different full cells at current densities of 1 C and 2 C.

4. Conclusion

In summary, an effective hybrid interfacial protective layer with organic (PVDF-HFP) and inorganic (Ag-Li_xAg_y) species was successfully prepared by in-situ reaction and sedimentation process on the Li foil. The organic-inorganic composite protective layer possesses outstanding Li^+ ion conductivity and excellent mechanical properties, which are beneficial to the uniform Li^+ ion transportation, the growth inhibition of Li dendrites, and the formation of "dead Li". During the charge-discharge process, the organic-inorganic composite film can maintain interfacial contact with Li foil and maintain superior structural stability. Thus, the pa-Li ‖ pa-Li symmetric cell delivers satisfactory stability and reversibility for 1000 h at a high current density of 5 mA cm^{-2} with a low voltage hysteresis of ~ 70 mV. The applicability of our design was further enhanced through the electrochemical performance of the full cells containing pa-Li anodes and $LiFePO_4$ cathodes, with the pa-Li ‖ LFP full cell exhibiting an impressive long-term stability for 900 cycles at 2 C, with a low capacity decay rate of 0.009% per cycle. Therefore, this work proposes a design protocol that enables the synergistic effect of PVDF-HFP organic species and Ag-Li_xAg_y inorganic species, thus providing a prospective way for the practical application of highly efficient, long lifespan Li metal anodes.

Acknowledgements

This work was financially supported by National Natural Science Foundation of China (Grant No. 51602200，61874074) and Singapore Ministry of Education academic research grant Tier 2 (T2EP50121-0007) and the 111 Project (D20015). Z. W. S. acknowledges the Agency for Science, Technology and Research (Central Research Fund Award).

Conflict of interest

The authors declare no conflict of interest.

Supporting Information

Supporting Information is available from the Wiley Online Library or from the author.

Corresponding Author

Bingbing Tian − International Collaborative Laboratory of 2D Materials for Optoelectronics Science and Technology of Ministry of Education, Institute of Microscale Optoelectronics, Shenzhen University, Shenzhen 518060, China; orcid.org/0000-0003-1508-6217; Email: tianbb2011@szu.edu.cn

Yumeng Shi − College of Electronics and Information Engineering, Shenzhen University, Shenzhen 518060, China; orcid.org/0000-0002-9623-3778; Email: yumeng.shi@szu.edu.cn

Hui Ying Yang − Pillar of Engineering Product Development, Singapore University of Technology and Design, Singapore 487372, Singapore; orcid.org/0000-0002-2244-8231; Email: yanghuiying@sutd.edu.sg

Reference

1. Yuan, H.; Ding, X.; Liu, T.; Nai, J.; Wang, Y.; Liu, Y.; Liu, C.; Tao, X., A review of concepts and contributions in lithium metal anode development. *Materials Today* **2022,** *53*, 173-196.

2. Jain, R.; Lakhnot, A. S.; Bhimani, K.; Sharma, S.; Mahajani, V.; Panchal, R. A.; Kamble, M.; Han, F.; Wang, C.; Koratkar, N., Nanostructuring versus microstructuring in battery electrodes. *Nature Reviews Materials* **2022,** *7* (9), 736-746.

3. Eng, A. Y. S.; Soni, C. B.; Lum, Y.; Khoo, E.; Yao, Z.; Vineeth, S. K.; Kumar, V.; Lu, J.; Johnson, C. S.; Wolverton, C.; Seh, Z. W., Theory-guided experimental design in battery materials research. *Sci Adv* **2022,** *8* (19), eabm2422.

4. Yan, D.; Yang, H. Y.; Bai, Y., Tactics to optimize conversion-type metal fluoride/sulfide/oxide cathodes toward advanced lithium metal batteries. *Nano Research* **2023,** DOI: 10.1007/s12274-023-5427-7.

5. Cheng, X.-B.; Zhang, R.; Zhao, C.-Z.; Zhang, Q., Toward Safe Lithium Metal Anode in Rechargeable Batteries: A Review. *Chemical Reviews* **2017,** *117* (15), 10403-10473.

6. Lin, D.; Liu, Y.; Cui, Y., Reviving the lithium metal anode for high-energy batteries. *Nature nanotechnology* **2017,** *12* (3), 194-206.

7. Deng, W.; Yin, X.; Bao, W.; Zhou, X. F.; Hu, Z. Y.; He, B. Y.; Qiu, B.; Meng, Y. S.; Liu, Z. P., Quantification of reversible and irreversible lithium in practical lithium-metal

batteries. *Nature Energy* **2022,** *7* (11), 1031-1041.

8. Yang, C.; Fu, K.; Zhang, Y.; Hitz, E.; Hu, L., Protected Lithium-Metal Anodes in Batteries: From Liquid to Solid. *Adv Mater* **2017,** *29*, 1701169.

9. Wang, L.; Zhou, Z.; Yan, X.; Hou, F.; Wen, L.; Luo, W.; Liang, J.; Dou, S. X., Engineering of lithium-metal anodes towards a safe and stable battery. *Energy Storage Materials* **2018,** *14*, 22-48.

10. Wei, C.; Zhang, Y.; Tian, Y.; Tan, L.; An, Y.; Qian, Y.; Xi, B.; Xiong, S.; Feng, J.; Qian, Y., Design of safe, long-cycling and high-energy lithium metal anodes in all working conditions: Progress, challenges and perspectives. *Energy Storage Materials* **2021,** *38*, 157-189.

11. Shi, Y.; Li, B.; Zhang, Y.; Cui, Y.; Cao, Z.; Du, Z.; Gu, J.; Shen, K.; Yang, S., Tortuosity Modulation toward High-Energy and High-Power Lithium Metal Batteries. *Advanced Energy Materials* **2021,** *11*, 2003663.

12. Horstmann, B.; Shi, J.; Amine, R.; Werres, M.; He, X.; Jia, H.; Hausen, F.; Cekic-Laskovic, I.; Wiemers-Meyer, S.; Lopez, J.; Galvez-Aranda, D.; Baakes, F.; Bresser, D.; Su, C.-C.; Xu, Y.; Xu, W.; Jakes, P.; Eichel, R.-A.; Figgemeier, E.; Krewer, U.; Seminario, J. M.; Balbuena, P. B.; Wang, C.; Passerini, S.; Shao-Horn, Y.; Winter, M.; Amine, K.; Kostecki, R.; Latz, A., Strategies towards enabling lithium metal in batteries: interphases and electrodes. *Energy & Environmental Science* **2021,** *14* (10), 5289-5314.

13. Liu, D.-H.; Bai, Z.; Li, M.; Yu, A.; Luo, D.; Liu, W.; Yang, L.; Lu, J.; Amine, K.; Chen, Z., Developing high safety Li-metal anodes for future high-energy Li-metal batteries: strategies and perspectives. *Chemical Society Reviews* **2020,** *49* (15), 5407-

5445.

14. Tikekar, M. D.; Choudhury, S.; Tu, Z.; Archer, L. A., Design principles for electrolytes and interfaces for stable lithium-metal batteries. *Nature Energy* **2016,** *1*, 1-7.

15. Guo, Y.; Li, H.; Zhai, T., Reviving Lithium-Metal Anodes for Next-Generation High-Energy Batteries. *Advanced Materials* **2017,** *29*, 1700007.

16. Yasin, G.; Arif, M.; Mehtab, T.; Lu, X.; Yu, D.; Muhammad, N.; Nazir, M. T.; Song, H., Understanding and suppression strategies toward stable Li metal anode for safe lithium batteries. *Energy Storage Materials* **2020,** *25*, 644-678.

17. Zhu, W.; Deng, W.; Zhao, F.; Liang, S.; Zhou, X.; Liu, Z., Graphene network nested Cu foam for reducing size of lithium metal towards stable metallic lithium anode. *Energy Storage Materials* **2019,** *21*, 107-114.

18. Zhao, F.; Zhou, X.; Deng, W.; Liu, Z., Entrapping lithium deposition in lithiophilic reservoir constructed by vertically aligned ZnO nanosheets for dendrite-free Li metal anodes. *Nano Energy* **2019,** *62*, 55-63.

19. Deng, W.; Zhu, W.; Zhou, X.; Zhao, F.; Liu, Z., Regulating capillary pressure to achieve ultralow areal mass loading metallic lithium anodes. *Energy Storage Materials* **2019,** *23*, 693-700.

20. Li, X. L.; Huang, S.; Yan, D.; Zhang, J.; Fang, D.; Lim, Y. V.; Wang, Y.; Li, T. C.; Li, Y.; Guo, L.; Yang, H. Y., Tuning Lithiophilicity and Stability of 3D Conductive Scaffold via Covalent Ag-S Bond for High-Performance Lithium Metal Anode. *Energy & Environmental Materials* **2022,** *6*, e12274.

21. Zhao, Q.; Zhou, R.; Wang, C.; Kang, J.; Zhang, Q.; Liu, J.; Jin, Y.; Wang, H.; Zheng, Z.; Guo, L., Anion Immobilization Enabled by Cation-Selective Separators for Dendrite-Free Lithium Metal Batteries. *Advanced Functional Materials* **2022,** 32, 2112711.

22. Han, D.; Wang, X.; Zhou, Y. N.; Zhang, J.; Liu, Z.; Xiao, Z.; Zhou, J.; Wang, Z.; Zheng, J.; Jia, Z.; Tian, B.; Xie, J.; Liu, Z.; Tang, W., A Graphene-Coated Thermal Conductive Separator to Eliminate the Dendrite-Induced Local Hotspots for Stable Lithium Cycling. *Advanced Energy Materials* **2022,** 12, 2201190.

23. Du, M.; Peng, Z.; Long, X.; Huang, Z.; Lin, Z.; Yang, J.; Ding, K.; Chen, L.; Hong, X. J.; Cai, Y. P.; Zheng, Q., Tuning the Metal Ions of Prussian Blue Analogues in Separators to Enable High-Power Lithium Metal Batteries. *Nano Lett* **2022,** 22, 12, 4861-4869.

24. Sun, S.; Wang, J.; Chen, X.; Ma, Q.; Wang, Y.; Yang, K.; Yao, X.; Yang, Z.; Liu, J.; Xu, H.; Cai, Q.; Zhao, Y.; Yan, W., Thermally Stable and Dendrite-Resistant Separators toward Highly Robust Lithium Metal Batteries. *Advanced Energy Materials* **2022,** *12*, 2202206.

25. Yu, Z.; Rudnicki, P. E.; Zhang, Z.; Huang, Z.; Celik, H.; Oyakhire, S. T.; Chen, Y.; Kong, X.; Kim, S. C.; Xiao, X.; Wang, H.; Zheng, Y.; Kamat, G. A.; Kim, M. S.; Bent, S. F.; Qin, J.; Cui, Y.; Bao, Z., Rational solvent molecule tuning for high-performance lithium metal battery electrolytes. *Nature Energy* **2022,** 7, 94-106.

26. Yin, Y.; Yang, Y.; Cheng, D.; Mayer, M.; Holoubek, J.; Li, W.; Raghavendran, G.; Liu, A.; Lu, B.; Davies, D. M.; Chen, Z.; Borodin, O.; Meng, Y. S., Fire-extinguishing,

recyclable liquefied gas electrolytes for temperature-resilient lithium-metal batteries. *Nature Energy* **2022,** 7, 548-559.

27. Zhao, Y.; Zhou, T.; Ashirov, T.; Kazzi, M. E.; Cancellieri, C.; Jeurgens, L. P. H.; Choi, J. W.; Coskun, A., Fluorinated ether electrolyte with controlled solvation structure for high voltage lithium metal batteries. *Nat Commun 13*, 2575 (2022).

28. Zhang, Q. K.; Zhang, X. Q.; Hou, L. P.; Sun, S. Y.; Zhan, Y. X.; Liang, J. L.; Zhang, F. S.; Feng, X. N.; Li, B. Q.; Huang, J. Q., Regulating Solvation Structure in Nonflammable Amide-Based Electrolytes for Long-Cycling and Safe Lithium Metal Batteries. *Advanced Energy Materials* **2022,** 12, 2200139.

29. Zhao, F.; Deng, W.; Dong, D.; Zhou, X.; Liu, Z., Seamlessly integrated alloy-polymer interphase for high-rate and long-life lithium metal anodes. *Materials Today Energy* **2022,** *26, 100988*.

30. Zhang, Z.; Guan, S. D.; Liu, S. J.; Hu, B. K.; Xue, C. J.; Wu, X. B.; Wen, K. H.; Nan, C. W.; Li, L. L., A Valence Gradient Protective Layer for Dendrite-Free and Highly Stable Lithium Metal Anodes. *Advanced Energy Materials* **2022**, 12, 2103332.

31. Yao, X.; Wang, J.; Lin, S.; Tao, C.; Zhang, X.; Wang, W.; Zhao, C.; Wang, L.; Bao, J. L.; Wang, Y.; Liu, T., Surface Bromination of Lithium-Metal Anode for High Cyclic Efficiency. *Advanced Energy Materials* **2022,** 13, 2203233.

32. Wang, Q.; Yang, J.; Huang, X.; Zhai, Z.; Tang, J.; You, J.; Shi, C.; Li, W.; Dai, P.; Zheng, W.; Huang, L.; Sun, S., Rigid and Flexible SEI Layer Formed Over a Cross-Linked Polymer for Enhanced Ultrathin Li Metal Anode Performance. *Advanced Energy Materials* **2022,** 12, 2103972.

33. Han, Z.; Zhang, C.; Lin, Q.; Zhang, Y.; Deng, Y.; Han, J.; Wu, D.; Kang, F.; Yang, Q. H.; Lv, W., A Protective Layer for Lithium Metal Anode: Why and How. *Small Methods* **2021,** *5* (4), e2001035.

34. Liu, H. J.; Yang, C. Y.; Han, M. C.; Yu, C. Y.; Li, X.; Yu, Z. Z.; Qu, J., In-Situ Constructing A Heterogeneous Layer on Lithium Metal Anodes for Dendrite-Free Lithium Deposition and High Li-ion Flux. *Angew Chem Int Ed Engl* **2023,** 62, e2022174.

35. Gao, S.; Sun, F.; Liu, N.; Yang, H.; Cao, P.-F., Ionic conductive polymers as artificial solid electrolyte interphase films in Li metal batteries – A review. *Materials Today* **2020,** *40*, 140-159.

36. Liang, X.; Pang, Q.; Kochetkov, I. R.; Sempere, M. S.; Huang, H.; Sun, X.; Nazar, L. F., A facile surface chemistry route to a stabilized lithium metal anode. *Nature Energy* **2017,** *2*, 17119.

37. Zhu, B.; Jin, Y.; Hu, X.; Zheng, Q.; Zhang, S.; Wang, Q.; Zhu, J., Poly(dimethylsiloxane) Thin Film as a Stable Interfacial Layer for High-Performance Lithium-Metal Battery Anodes. *Advanced Materials* **2017,** *29*, 1603755.

38. Lopez, J.; Pei, A.; Oh, J. Y.; Wang, G. N.; Cui, Y.; Bao, Z., Effects of Polymer Coatings on Electrodeposited Lithium Metal. *J Am Chem Soc* **2018,** *140* (37), 11735-11744.

39. Yan, C.; Cheng, X.-B.; Tian, Y.; Chen, X.; Zhang, X.-Q.; Li, W.-J.; Huang, J.-Q.; Zhang, Q., Dual-Layered Film Protected Lithium Metal Anode to Enable Dendrite-Free Lithium Deposition. *Advanced Materials* **2018,** *30*, 1707629.

40. Chen, C.; Liang, Q.; Wang, G.; Liu, D.; Xiong, X., Grain-Boundary-Rich Artificial SEI Layer for High-Rate Lithium Metal Anodes. *Advanced Functional Materials* **2021,** *32*, 2107249.

41. Hu, Z.; Zhang, S.; Dong, S.; Li, W.; Li, H.; Cui, G.; Chen, L., Poly(ethyl α-cyanoacrylate)-Based Artificial Solid Electrolyte Interphase Layer for Enhanced Interface Stability of Li Metal Anodes. *Chemistry of Materials* **2017,** *29* (11), 4682-4689.

42. Li, S.; Wang, X.-S.; Li, Q.-D.; Liu, Q.; Shi, P.-R.; Yu, J.; Lv, W.; Kang, F.; He, Y.-B.; Yang, Q.-H., A multifunctional artificial protective layer for producing an ultra-stable lithium metal anode in a commercial carbonate electrolyte. *Journal of Materials Chemistry A* **2021,** *9* (12), 7667-7674.

43. Zhao, K.; Zhang, L.; Jin, Q.; Xiao, J.; Wu, L.; Zhang, X., Tuning Li Nucleation by a Hybrid Lithiophilic Protective Layer for High-Performance Lithium Metal Batteries. *ACS Appl Mater Interfaces* **2023,** 15, 2, 3089-3098.

44. Liu, T.; Hu, Q.; Li, X.; Tan, L.; Yan, G.; Wang, Z.; Guo, H.; Liu, Y.; Wu, Y.; Wang, J., Lithiophilic Ag/Li composite anodes via a spontaneous reaction for Li nucleation with a reduced barrier. *Journal of Materials Chemistry A* **2019,** *7* (36), 20911-20918.

45. Cao, W.; Lu, J.; Zhou, K.; Sun, G.; Zheng, J.; Geng, Z.; Li, H., Organic-inorganic composite SEI for a stable Li metal anode by in-situ polymerization. *Nano Energy* **2022,** *95, 106983*.

46. Guo, Z.; Zhang, Q.; Wang, C.; Zhang, Y.; Dong, S.; Cui, G., I-containing Polymer/Alloy Layer-Based Li Anode Mediating High-Performance Lithium–Air

Batteries. *Advanced Functional Materials* **2021,** *32*, 2108993.

47. Zhang, S.; Yang, G.; Liu, Z.; Weng, S.; Li, X.; Wang, X.; Gao, Y.; Wang, Z.; Chen, L., Phase Diagram Determined Lithium Plating/Stripping Behaviors on Lithiophilic Substrates. *ACS Energy Letters* **2021,** *6* (11), 4118-4126.

48. Fang, Y.; Zhang, S. L.; Wu, Z. P.; Luan, D.; Lou, X. W. D., A highly stable lithium metal anode enabled by Ag nanoparticle-embedded nitrogen-doped carbon macroporous fibers. *Sci Adv* **2021,** *7*, eabg3626.

49. Li, L.; Fu, H.; Yang, J.; Wang, P.; Zhang, H.; Zhao, X.; Xiao, Z.; Liu, Z.; Kou, Z.; Wang, Z.; He, D., A dual-confined lithium nucleation and growth design enables dendrite-free lithium metal batteries. *Journal of Materials Chemistry A* **2022,** 10, 11659-11656.

50. Wang, X.; Pan, Z.; Wu, Y.; Xu, G.; Zheng, X.; Qiu, Y.; Liu, M.; Zhang, Y.; Li, W., Reducing lithium deposition overpotential with silver nanocrystals anchored on graphene aerogel. *Nanoscale* **2018,** *10* (35), 16562-16567.